International Journal of Thermophysics, Vol. 26, No. 3, May 2005 (© 2005)
DOI: 10.1007/s10765-005-5586-2

Transient Free Convection Fluid Flow in a Vertical Microchannel as Described by the Hyperbolic Heat Conduction Model

A. F. Khadrawi,[1,2] Ali Othman,[3] and M. A. Al-Nimr[4]

Received September 6, 2004

The transient hydrodynamics and thermal behaviors of fluid flow in an open-ended vertical parallel-plate microchannel are investigated analytically under the effect of the hyperbolic heat conduction model. The model that combines both the continuum approach and the possibility of slip at the boundary is adopted in this study. The effects of Knudsen number Kn and thermal relaxation time τ on the microchannel hydrodynamics and thermal behaviors are investigated using the hyperbolic and the parabolic heat conduction models. It is found that as Kn increases, the slip in the hydrodynamic and thermal boundary condition increases. Also, this slip increases as τ decreases.

KEY WORDS: free convection; hyperbolic heat conduction; macroscopioc heat conduction models in microchannel; vertical microchannel; microchannel thermal and hydrodynamic behavior.

1. INTRODUCTION

Recently, a growing interest in microchannel fluid mechanics and heat transfer has emerged because of possible cooling applications in space systems, manufacturing and material processing operations, and in high-power-density chips in supercomputers and other electronics. As this area continues to grow, it becomes increasingly important to understand the

[1] Mechanical Engineering Department, Al-Balqa' Applied University, Al-Huson College, P.O. Box 50, Irbid 21510, Jordan.
[2] To whom correspondence should be addressed. E-mail: khadrawi99@yahoo.com
[3] Mechanical Engineering Department, Philadelphia University, Jordan.
[4] Mechanical Engineering Department, Jordan University of Science and Technology, P.O. Box 3030, Irbid 22110, Jordan.

mechanisms and fundamental differences involved with fluid mechanics and heat transfer in microchannels.

It has been reported that the phenomena in microgeometry may differ from those in macroscopic counterparts. Several factors that are dominant at the microscale have been identified through a number of experimental, analytical, and numerical studies. Among them, the non-continuum effect, the compressibility effect, and various surface effects have been under vigorous investigation. In microgeometries the flow is described as granular for liquids and rarefied for gases, and the walls "move" [1]. The approximations for continuum flow analysis fail for microscale flows as the characteristic length of the flow gradients (L) approaches the average distance traveled by molecules between collisions (mean free path, λ). The ratio of these quantities is known as the Knudsen number ($Kn = \lambda/L$) and is used to indicate the degree of flow rarefaction or the scale of flow problem. Rarefaction or microscale effects are ignored by the Navier–Stokes equations, and these equations are therefore strictly accurate only at a vanishingly small Kn ($Kn < 0.001$). The appropriate flow and heat transfer models depend on the range of the Knudsen number, and a classification of the different gas flow regimes is as follows: $Kn < 0.001$ for continuum flow, $0.001 < Kn < 0.1$ for slip flow, $0.1 < Kn < 10$ for transition flow, and $10 < Kn$ for free molecular flow [2].

In the slip flow regime, the continuum flow model is still valid for calculations of the flow properties away from solid boundaries. However, the boundary conditions have to be modified to account for the incomplete interactions between the gas molecules and the solid boundaries. The important features of gas flow in micro ducts are mainly due to rarefaction and compressibility effects. Two more effects due to acceleration and non-parabolic velocity profile were found to be of second order compared to the compressibility effect [3]. The rarefaction effect can be studied by solving the momentum and energy equations with slip velocity and temperature jump boundary conditions.

In spite of the large number of published research so far in the microflow literature (for more details, the reader may refer to the following review papers [4, 5]) many parts of the physical laws governing the fluid flow and heat transfer in microgeometry remain unknown. Recently, discrepancies between microchannel flow behavior and macroscale Stokes flow theory have been summarized in a review [6]. It is widely accepted that the deviation observed in gas flows can be attributed to slip at the wall [7], and several researchers have reported results for gas flows [8–12].

In parallel to the breakdown of the continuum flow approach and the no-slip boundary condition from hydrodynamics and thermal point of view, the classical diffusion energy equation, based on Fourier's law, does

not apply well in the microdevices. The thermal behavior of microchannels has been extensively investigated by many researchers using different models, design, and geometrical and operating parameters. Most of these studies are based on the parabolic (diffusion) heat conduction model. The parabolic heat conduction model is able to describe the thermal behavior of these microchannels in many practical applications. However, there are numerous cases in which the utilization of the hyperbolic heat conduction model becomes essential [13–21]. Examples of these cases are very fast transient heat conduction processes, heat conduction at cryogenic temperatures, high heating rate processes, and situations involving high temperature gradients similar to heat found in microsystems. In these applications, lagging is expected to occur between the heat flux and the temperature gradient across the fluid domain. Cattaneo [14] and Vernotte [15] suggested independently a modified heat flux model in the form,

$$\vec{q}\,(t+\bar{\tau},\vec{r}) = -k\vec{\nabla}T\,(t,\vec{r}) \tag{1}$$

where $\vec{q}$ is the heat flux vector, k is the thermal conductivity, $\vec{r}$ is a special vector, and $\bar{\tau}$ is the phase-lag in the heat flux vector. The constitutive law of Eq. (1) assumes that the heat flux vector (the effect) and the temperature gradient (the cause) across a material volume occur at different instants of time, and the time delay between the heat flux and the temperature gradient is the relaxation time $\bar{\tau}$.

In the absence of the phase-lag in the heat flux vector ($\bar{\tau} = 0$), Eq. (1) reduces to the classical diffusion equation employing Fourier's law. Due to this lagging response, the hyperbolic heat conduction models have been receiving increasing attention as compared to the classical diffusion model, which assumes an immediate response between the heat flux vector and the temperature gradient.

The objective of this study is to investigate the microchannel transient behavior under the effect of the hyperbolic heat conduction model. The model that combines the continuum approach with slip at the boundaries is adopted in this investigation. The effects of the Knudsen number and the phase-lag in heat flux on the deviations between the two heat conduction models are investigated.

2. ANALYSIS

Consider an unsteady laminar fully developed free convection flow inside an open-ended vertical parallel-plate microchannel. The fluid is assumed to be Newtonian with uniform properties. Also, it is assumed that both viscous dissipation and internal heat generation are absent. Referring

to Fig. 1 and using the dimensionless parameters given in the nomenclature, the governing equations of the hydrodynamic and thermal behaviors, as described by the hyperbolic heat conduction model, are given as [16]

$$\frac{\partial U}{\partial \eta} = \theta + \frac{\partial^2 U}{\partial Y^2} \tag{2}$$

$$\frac{\partial \theta}{\partial \eta} = -\frac{1}{Pr}\frac{\partial Q}{\partial Y} \tag{3}$$

$$Q + \tau \frac{\partial Q}{\partial \eta} = -\frac{\partial \theta}{\partial Y} \tag{4}$$

Equations (2)–(4) assume the following initial and boundary thermal conditions:

$$\theta\,(0, Y) = U\,(0, Y) = 0 \tag{5a}$$

$$U\,(\eta, 1) = -H\,Kn \frac{\partial U}{\partial Y}\,(\eta, 1) \tag{5b}$$

$$\frac{\partial U}{\partial Y}\,(\eta, 0) = 0 \tag{5c}$$

$$\frac{\partial \theta}{\partial Y}\,(\eta, 0) = 0 \tag{5d}$$

$$\theta\,(\eta, 1) - 1 = Kn \frac{\psi}{Pr} Q\,(\eta, 1) \tag{5e}$$

where $H = \frac{2-\sigma_v}{\sigma_v}$, $\psi = \frac{2-\sigma_T}{\sigma_T}\left(\frac{2\gamma}{\gamma+1}\right)$, γ is the specific heat ratio, σ_T is the thermal accommodation coefficient, σ_v is the tangential-momentum accommodation coefficient, and $Kn = \frac{\lambda}{L}$ (Knudson number).

Also, the dimensionless slip-flow and temperature jump boundary conditions are given as, respectively,

$$\Delta U|_{\text{wall}} = U\,(\eta, 1) = -H\,Kn \frac{\partial U}{\partial Y}\,(\eta, 1)\,,$$

$$\Delta \theta|_{\text{wall}} = \theta\,(\eta, 1) - 1 = Kn \frac{\psi}{Pr} Q\,(\eta, 1)$$

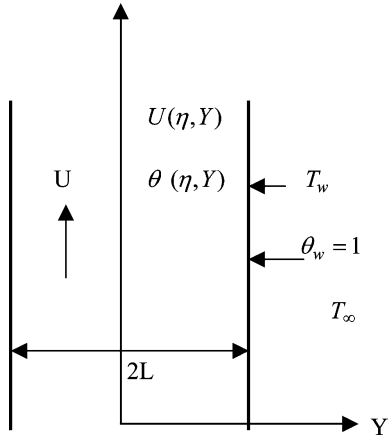

Fig. 1. Schematic diagram of the problem under consideration.

where the right-hand side of Eqs. (5b) and (5e) represents the slip in the hydrodynamic and thermal boundary condition.

Equations (2)–(5) are solved using the Laplace transformation technique. Now with the notation that $L\{\theta(\eta, Y)\} = W(S, Y)$, $L\{Q(\eta, Y)\} = V(S, Y)$, and $L\{U(\eta, Y)\} = F(S, Y)$, the Laplace transformation of Eqs. (2)–(5) yields

$$S F = W + \frac{d^2 F}{dY^2} \tag{6}$$

$$S W = -\frac{1}{Pr}\frac{dV}{dY} \tag{7}$$

$$V + \tau S V = -\frac{dW}{dY} \tag{8}$$

Also, the Laplace transformation of the boundary conditions is given as

$$\frac{\partial F}{\partial Y}(S, 0) = 0$$

$$F(S, 1) = -H Kn \frac{\partial F}{\partial Y}(S, 1) \tag{9}$$

$$\frac{\partial W}{\partial Y}(S, 0) = 0$$

$$W(S,1) - \frac{1}{s} = Kn\frac{\psi}{Pr} V(S,1)$$

According to the boundary conditions given in Eq. (9), Eqs. (6)–(8) are solved to give

$$W = \frac{-C}{S\,Pr}\beta \cosh(\beta Y) \tag{10}$$

$$V = C \sinh(\beta Y) \tag{11}$$

$$F = C_1 \cosh(\sqrt{S}Y) + C_2 \cosh(\beta Y) \tag{12}$$

where

$$C = \frac{-1/S}{\left[\frac{\beta}{S\,Pr}\cosh(\beta) + Kn\frac{\psi}{Pr}\sinh(\beta)\right]}, \quad C_2 = \frac{C\beta}{\left[(\beta^2 - S)\,S\,Pr\right]},$$

$$C_1 = \frac{-C_2\left[\cosh(\beta) + H\,Kn\,\beta\sinh(\beta)\right]}{\left[\cosh\left(\sqrt{S}\right) + H\,Kn\sqrt{S}\sinh\left(\sqrt{S}\right)\right]}, \quad \textit{and} \quad \beta = \sqrt{S\,Pr\,(1+\tau\,S)}.$$

Equations (10)–(12) are inverted in terms of the Riemann-sum approximation [13] as

$$\theta(\eta, Y) \cong \frac{e^{\varepsilon\eta}}{\eta}\left[\frac{1}{2}W(\varepsilon, Y) + \mathrm{Re}\sum_{n=1}^{N} W\left(\varepsilon + \frac{in\pi}{\eta}, Y\right)(-1)^n\right] \tag{13}$$

where Re refers to the "real part of" and $i = \sqrt{-1}$ is the imaginary number, N is the number of terms used in the Riemann-sum approximation, and ε is the real part of the Bromwich contour that is used in inverting Laplace transforms. The Riemann-sum approximation for the Laplace inversion involves a single summation for the numerical process. Its accuracy depends on the value of ε and the truncation error dictated by N. The value of ε must be selected so that the Bromwich contour encloses all the branch points [1]. For faster convergence, however, numerous numerical experiments have shown that a value satisfying the relation $\varepsilon\eta \cong 4.7$ gives the most satisfactory results [15]. Hence, the appropriate value of ε for faster convergence depends on the instant of time (η) at which the lagging phenomenon is studied. The criterion shown by $\varepsilon\eta \cong 4.7$ is independent of the value of η. The number N of terms used in the Riemann-sum is determined. Thus, a prescribed threshold for the accumulated partial sum is satisfied at given values of ε, Y, and η.

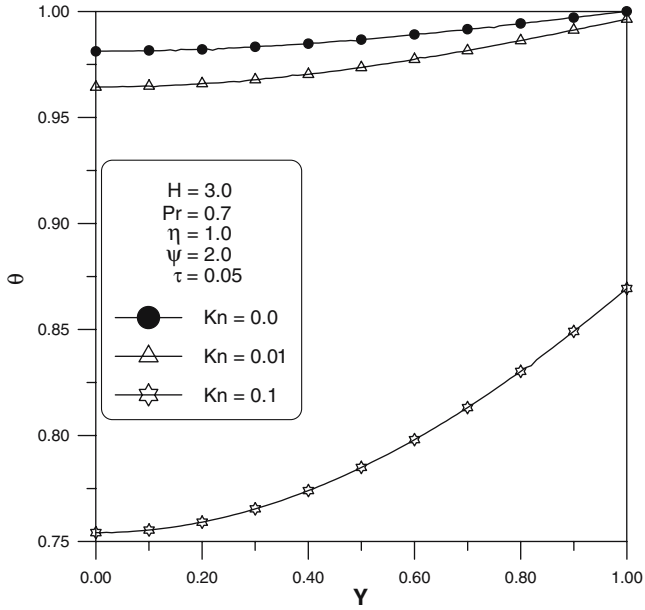

Fig. 2. Spatial temperature distribution at different *Kn*.

3. RESULTS AND DISCUSSION

Figure 2 shows the effect of the Knudsen number *Kn* on the spatial temperature distribution. As shown from this figure, an increase in *Kn* yields an increase in the temperature jump at the heated wall. This is due to the reduction in the interaction between the gas molecules and the heated wall. As the *Kn* number increases, the mean free path length of the gas molecules increases which implies that any molecule reflected from the wall has less opportunity to collide with other molecules and then to transmit it to the wall heating effect. A larger *Kn* implies fewer molecules collide with the wall and carry part of its heating effect. As a result of an increase in the temperature jump at the wall, less heat is transmitted to the gas, which yields less buoyancy driving force. This produces low temperature profiles at higher *Kn* as observed from Fig. 2.

The effect of the thermal relaxation time on the temperature spatial distribution is shown in Fig. 3. An increase in the thermal relaxation time τ yields an increase in the gas temperature, especially at a location far away from the heated wall. As a result, any increase in τ yields an increase in the temperature distribution at the same time. Although the classical wave model predicts a temperature disturbance propagating as a

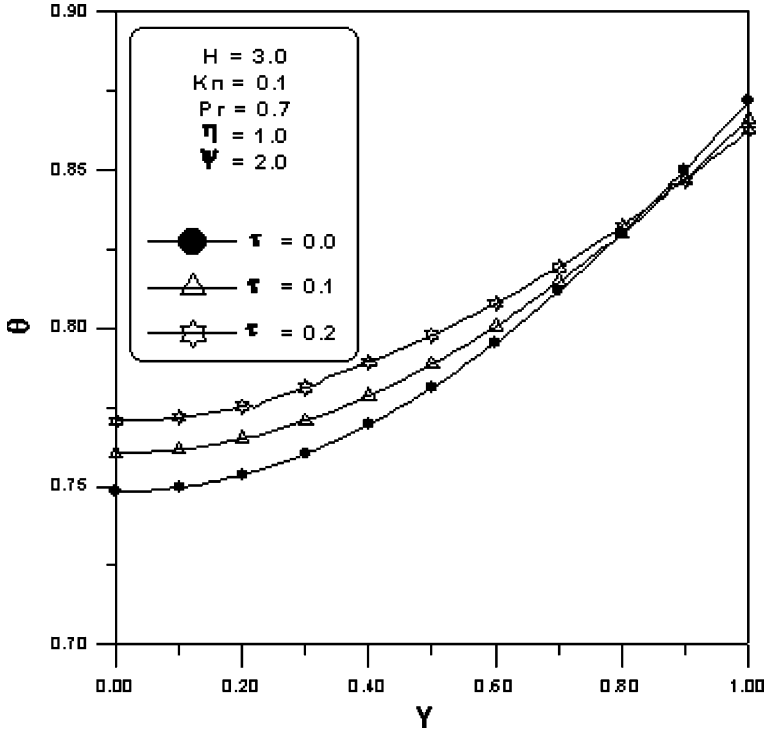

Fig. 3. Spatial temperature distribution at different τ.

wave, with the thermal diffusivity appearing as a damping effect in heat propagation, it also accounts for the increase of the heat flux vector due to the phonon collision in a duration of the mean free time τ. Note that in Fig. 3, $\tau = 0$ represents the classical diffusion model and other values of τ are for the hyperbolic wave model. The fact that the wave model predicts a higher temperature than the diffusion model is clear in other examples considered in Ref. 13. A mathematical justification for the behavior shown in Fig. 3 may be approached by writing the energy equation in terms of temperature as described by the hyperbolic heat conduction model. This equation may be written as

$$\rho c \frac{\partial T}{\partial t} + \rho c \tau \frac{\partial^2 T}{\partial t^2} = k \frac{\partial^2 T}{\partial y^2} \tag{14}$$

Due to the downward concavity of the dynamic temperature profile, the second term in Eq. (14) has a negative sign. This negative sign reduces

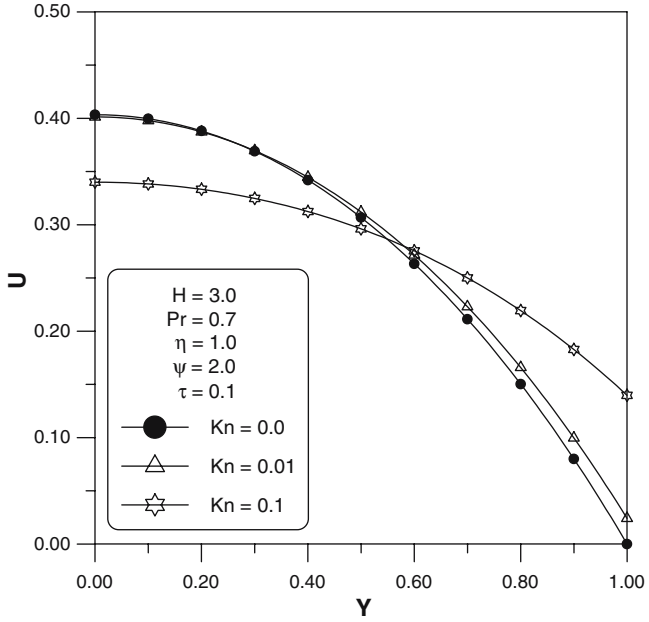

Fig. 4. Spatial velocity distribution at different *Kn*.

the effective thermal storage of the domain. As a result, any amount of heat transfer produces a higher temperature within the domain.

Figure 4 shows the effect of *Kn* on the velocity spatial distribution. As *Kn* increases, the velocity slip at the wall increases which reduces the retarding effect of the wall. This yields an observable increase in the gas velocity near the wall. However, as *Kn* increases, the temperature jump increases and this reduces the amount of heat transfer from the wall to the fluid. This reduction in heat transfer reduces the buoyancy effect, which drives the flow and hence reduces the gas velocity far from the wall. The reduction in velocity due to the reduction in heat transfer is offset by the increase in U due to the reduction in the frictional retarding forces near the wall. The effect of the thermal relaxation time τ on the velocity spatial distribution is shown in Fig. 5. The figure shows an observable reduction in the gas velocity as τ increases. The justification for this behavior is discussed previously by explaining the effect of τ on the spatial temperature distribution.

The effect of *Kn* on the transient behavior of the wall temperature jump is shown in Fig. 6. It is clear that the temperature jump increases as *Kn* increases as explained previously. Also, it is clear that the temperature

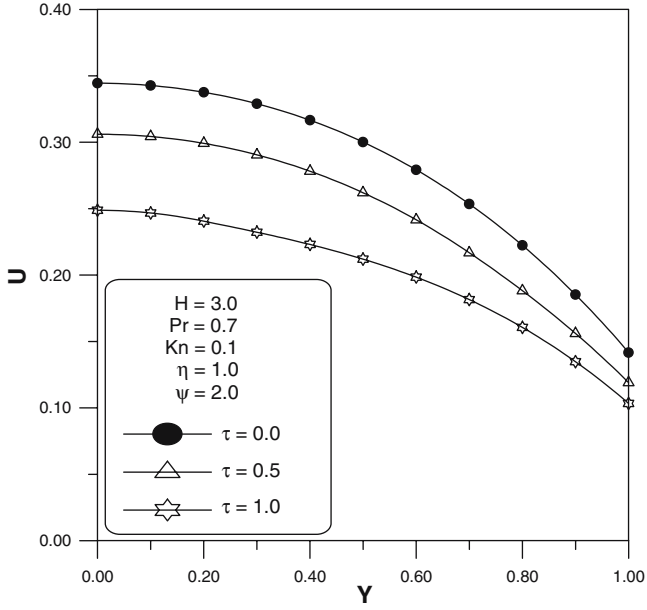

Fig. 5. Spatial velocity distribution at different τ.

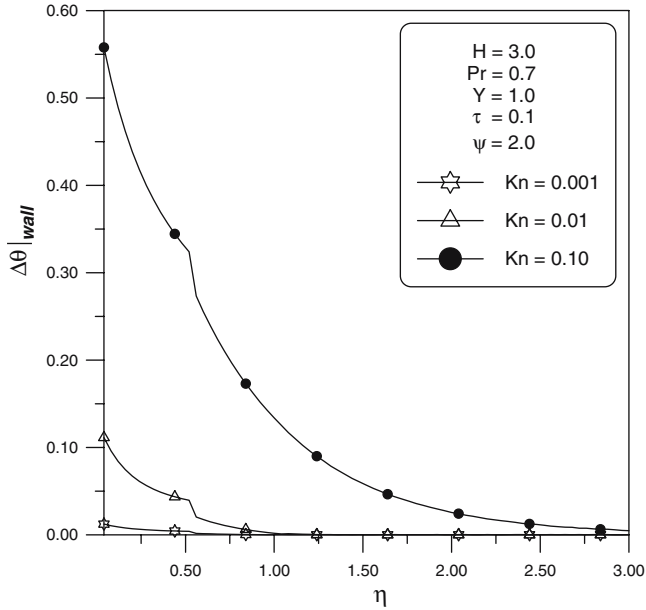

Fig. 6. Effect of *Kn* on the transient temperature difference at the wall.

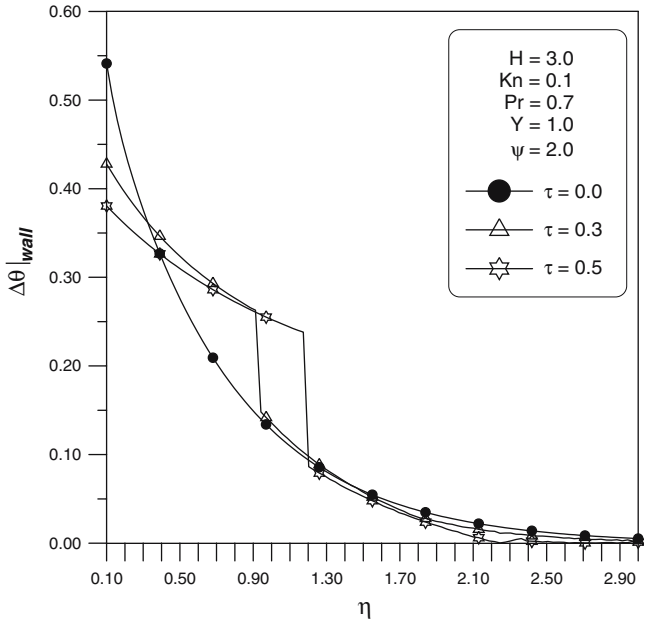

Fig. 7. Effect of τ on the transient temperature difference at the wall.

jump decreases as time proceeds and then approaches a very small, but non-zero, asymptote especially at large values of *Kn*. As time proceeds, the heating effect of the wall raises the gas temperature and the difference between the wall and the adjacent gas temperatures decreases.

The effect of τ on the transient behavior of the wall temperature jump is shown in Fig. 7. It is clear that the temperature jump decreases as time proceeds as explained in Fig. 6. The effect of τ is significant within the early stages of time. The discontinuities observed in Figs. 6 and 7 are due to the presence of τ in the momentum equation, which makes it hyperbolic in nature. This implies that the hydrodynamic behavior propagates as waves with abrupt changes. In fact, the presence of the second time derivative in the wave equation enforces the thermal disturbance to propagate as a wave with a moving front. The thermal diffusivity appearing in the wave model acts as a damping effect, which reduces this discontinuity a little.

The effect of *Kn* on the transient behavior of the velocity slip at the wall is shown in Fig. 8. As predicted, the velocity slip increases as *Kn* increases and as time proceeds. As time proceeds, the gas temperature increases and raises the gas velocity due to the buoyancy effect. As a

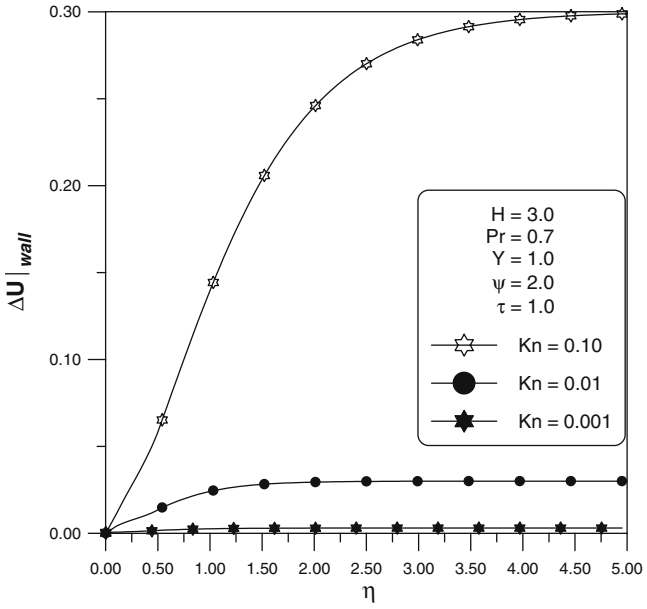

Fig. 8. Effect of *Kn* on the transient velocity difference at the wall.

result, the difference between the adjacent gas velocity and the wall zero velocity increases. Also, it is clear that flow needs more time to reach the steady-state behavior as *Kn* increases.

4. CONCLUSIONS

The transient hydrodynamics and thermal behaviors of fluid flow in an open-ended vertical parallel-plate microchannel are investigated analytically under the effect of the hyperbolic heat conduction model. Microchannel hydrodynamics and thermal behaviors are affected by two parameters, *Kn* and τ. It is found that as *Kn* increases the slip in the hydrodynamic and thermal boundary condition increases. Also, this slip increases as τ decreases.

NOMENCLATURE

c specific heat, $J \cdot kg^{-1} \cdot K^{-1}$
F Laplace transformation of the dimensionless velocity
H $= \frac{2-\sigma_v}{\sigma_v}$
Kn Knudsen number, λ/L

k thermal conductivity, $\mathrm{W{\cdot}m^{-1}{\cdot}K^{-1}}$
L characteristic length, m
Pr Prandtl number, ν/α
q conduction heat flux, $\mathrm{W{\cdot}m^{-2}}$
q_o reference conduction heat flux, $k\,\Delta T/L$
Q dimensionless conduction heat flux, q/q_o
$\vec{r}$ special vector, m
S Laplacian domain
t time, s
T temperature, K
T_∞ ambient and initial temperature, K
T_w wall temperature, K
u axial velocity, $\mathrm{m{\cdot}s^{-1}}$
u_o reference velocity, $L^2 g\beta\,(T_\mathrm{w}-T_\infty)/\nu$
U dimensionless velocity, u/u_o
V Laplace transformation of the dimensionless heat flux
W Laplace transformation of the dimensionless temperature
y transverse coordinate, m
Y dimensionless transverse coordinate, y/L

Greek symbols

α thermal diffusivity, $\mathrm{m^2{\cdot}s^{-1}}$
ΔT dimensionless temperature difference, $T_\mathrm{w}-T_\infty$
ψ $\frac{2-\sigma_\mathrm{T}}{\sigma_\mathrm{T}}\left(\frac{2\gamma}{\gamma+1}\right)$
η dimensionless time, $\nu t/L^2$
γ specific heat ratio
λ mean free path, m
ν kinematic viscosity, $\mathrm{m^2{\cdot}s^{-1}}$
ρ density, $\mathrm{kg{\cdot}m^{-3}}$
σ_v tangential-momentum accommodation coefficient
σ_T thermal accommodation coefficient
θ dimensionless temperature, $(T-T_\infty)/(T_\mathrm{w}-T_\infty)$
$\bar{\tau}$ phase-lag in heat flux vector, s
τ dimensionless phase-lag in heat flux vector, $\bar{\tau}_q\,\alpha/L^2$

Subscript

∞ ambient
w wall

REFERENCES

1. G. Karniadakis and A. Beskok, *Micro-flows Fundamentals and Simulation* (Springer-Verlag, New York, 2002).
2. Y. Zohar, *Heat Convection in Micro Ducts* (Kluwer, Boston, 2003).
3. Y. Zohar, W. Lee, S. Lee, L. Jiang, and P. Tong, *J. Fluid Mech.* **472:**125 (2002).
4. G. P. Duncan and G. P. Peterson, *Applied Mech. Rev.* **47:**397 (1994).
5. N. T. Obot, *Microscale Thermophys. Eng.* **6:**155 (2002).
6. C. Ho and Y. Tai, *Annu. Rev. Fluid Mech.* **30:**579 (1998).
7. J. C. Shih, C. Ho, J. Liu, and Y. Tai, *Microelectromech. Syst.* (MEMS) **59:**197 (1996).
8. P. Wu and W. A. Little, *Cryogenics* **23:**273 (1983).
9. S. B. Choi, R. F. Barron, and O. R. Warrington, *Micromech. Sensors, Actuators, Syst.* **32:**123 (1991).
10. J. C. Harley, Y. Huang, H. Bau, and J. N. Zemel, *J. Fluid Mech.* **284:**257 (1995).
11. S. F. Choquette, M. Faghri, E. J. Kenyon, and B. Sunden, *Proc. Nat. Heat Transfer Conf.* **5:**25 (1996).
12. Z. Y. Guo and X. B. Wu, *Int. J. Heat Transfer* **40:**3251 (1997).
13. D. Y. Tzou, *Macro to Microscale Heat Transfer, The Lagging Behavior* (Taylor and Francis, 1997).
14. C. Cattaneo, *Compte Rendus* **247:**431 (1958).
15. P. Vernotte, *Compte Rendus* **25:**2190 (1961).
16. D. Y. Tzou, *ASME J. Heat Transfer* **117:**8 (1995a).
17. D. Y. Tzou, *Int. J. Heat Mass Transfer* **38:**3231 (1995b).
18. D. Y. Tzou, *AIAA J. Thermophys. Heat Transfer* **9:**686 (1995c).
19. M. A. Al-Nimr and M. Naji, *Int. J. Thermophys.* **21:**281 (2000).
20. M. A. Al-Nimr and M. Naji, *Microscale Thermophys. Eng.* **4:**231 (2000b).
21. M. A. Al-Nimr, M. Naji, and V. Arpaci, *ASME J. Heat Transfer* **122:**217 (2000).